ORNL/TM-2022/2430

Collection of Aerosol Particles in a Single-Stage, High-Gradient Magnetic Collector

Shannon M. Mahurin
Meng-Dawn Cheng
Paula R. Cable-Dunlap

April 2022

OAK RIDGE National Laboratory

ORNL IS MANAGED BY UT-BATTELLE LLC FOR THE US DEPARTMENT OF ENERGY

ORNL/TM-2022/2430

Environmental Sciences Division

COLLECTION OF AEROSOL PARTICLES IN A SINGLE-STAGE, HIGH-GRADIENT MAGNETIC COLLECTOR

Shannon M. Mahurin
Meng-Dawn Cheng
Paula R. Cable-Dunlap

April 2022

Prepared by
OAK RIDGE NATIONAL LABORATORY
Oak Ridge, TN 37831
managed by
UT-BATTELLE LLC
for the
US DEPARTMENT OF ENERGY
under contract DE-AC05-00OR22725

CONTENTS

LIST OF FIGURES

ABBREVIATIONS

APS	Aerodynamic Particle Sizer
Fe_3O_4	Iron Oxide
GSD	Geometric Standard Deviation
HGMS	High-Gradient Magnetic Separation
HGPMS	High-Gradient Permanent Magnetic Separation
LPM	Liters Per Minute
NaCl	Sodium Chloride
NdFeB	Neodynium Iron Boron
Ni	Nickel
NMAC	Non-Magnetic Aerosol Collector
ORNL	Oak Ridge National Laboratory
PMAC	Permanent Magnet Aerosol Collector
PM10	Particulate Matter of Aerodynamic Diameter of 10 Microns or Less
SEM	Scanning Electron Microscope
SiO_2	Silicon Dioxide
SMPS	Scanning Mobility Particle Sizer
UAS	Unmanned Aerial System

ABSTRACT

The collection of aerosol particles that have magnetic components such as actinides, cobalt, iron, nickel, and other metal alloys are of interest in the nuclear industry and for regulatory applications. The collection of these particles is important for environmental monitoring and source location and approaches have been developed based on separations mechanisms including size, mass, electrical or thermal properties. In this work, we present the performance of a single-stage, high-gradient magnetic collector with a nickel foam matrix for removing airborne magnetic particles. The collection efficiencies for two different particle size regimes and compositions (NaCl and Fe_3O_4 below 200 nm and SiO_2 and Fe_3O_4 at 1-2 μm) were measured to assess the performance of the magnetic collector. The high-gradient magnetic collector did not remove nanosized magnetic Fe_3O_4 particles any more effectively than non-magnetic NaCl particles. However, in the larger size range, the collector more efficiently removed Fe_3O_4 particles compared to SiO_2 with a collection efficiency of 99% compared to 84% for SiO_2. The removal mechanism could be attributed to both filtration and the high-gradient magnetic field.

1. INTRODUCTION

The recovery and removal of micron-sized and larger magnetic particles from slurries and air streams by high-gradient magnetic separation (HGMS) has been employed since the early 1970s.[1-6] Though there has been significant work in the area of liquid-based magnetic particle separation from colloidal suspensions for industry and for environmental separations,[7, 8] the collection of airborne particles using magnetic susceptibility has been much less explored.[9, 10] The collection of airborne particulate matter or aerosol particles using magnetic separation technology is of broad interest for industrial and regulatory applications[1, 11-17] because aerosol particles are ubiquitous in the environment, and many have magnetic components which makes it possible to use magnetic separation for particle collection.

Work utilizing the magnetic properties of aerosols to distinguish particles from vehicle traffic and industrial sources in Wuhan, China[18] suggested that magnetic measurements could be used to map heavy metal pollution and provide insight into the pollutant source in road dust. Sagnotti et al. reported magnetic fingerprints associated with sources of natural and anthropogenic particulate matter of 10 μm in aerodynamic diameter (PM10).[19] The magnetic signature in airborne pollution particles in both the city center and suburbs of Warsaw, Poland has also been used to distinguish the source contribution of different particle size fractions.[20] While a variety of aerosol collectors that separate and collect particles based on size, mass, electrical, and/or thermal properties have been developed,[21] few have taken advantage of the magnetic components of airborne particles for selective collection,[22] which could enhance the performance of aerosol collection. In a magnetic collector, particles are separated based on both their size and magnetic susceptibility, simultaneously.[16, 17]

A recent example of the development of a passive aerosol sampler using permanent magnets was reported by Hsiao et al.[23] The sampler used 186 small magnets arranged in an alternating pole configuration to collect particles as they deposited onto the collection substrate though no collection efficiency data were reported.[23] An active aerosol sampler designed using a 3-stage high-gradient permanent magnetic separation (HGPMS) array was first reported by Cheng et al.[16] The authors demonstrated the effective capture of nanoparticles by configuring the permanent magnets as reversed pole pairs and adding a paramagnetic matrix such as stainless-steel wool to create the high-gradient magnetic field. The results were compared to those reported earlier.[10, 24] Cheng et al. further explored permanent magnet collection in a subsequent report and concluded that while the presence of a matrix is important in the capture of small nanoparticles (<50 nm), the design of the matrix is also critical to achieve high particle collection efficiencies across a broad range of particle sizes.[17] The disadvantage is that these magnetic collectors are

heavy and the design is cumbersome. As a result, they fail to meet the requirements of airborne particle collection based on an unmanned aerial system (UAS) such as a fixed- or rotating-wing drone.

This paper presents the development and testing results of a single-stage HGPMS collector for airborne particles. The single-stage magnet design was a revision of the previous 3-stage magnetic collectors resulting in a reduced weight of the collection system by at least 70% and a reduced overall footprint of 80%. Thus, it has the advantages of meeting operational requirements on a UAS. However, the design also significantly reduces the particle residence time and magnetic field strength distribution thereby affecting the collection performance. To explore the performance of the single-stage magnetic collector, we measured the collection efficiency of the collector for both supermicron-sized Fe_3O_4 and SiO_2 particles as well as smaller, nano-sized Fe_3O_4 and NaCl particles. Comparing the collection efficiency of the collector using both magnetic and non-magnetic particles allowed us to isolate the effect of the magnetic susceptibility on particle collection. Two different size regimes were used because the magnetic force experienced by aerosol particles is proportional to the particle volume (hence the diameter). The new design could lead to smaller, more efficient collectors that could be used in unmanned aerial systems.

2. EXPERIMENTAL

2.1 DESCRIPTION OF THE AEROSOL COLLECTOR

In previous work, the authors reported the performance of a permanent magnetic collector in which permanent magnets were arranged in an opposing polarity configuration and enclosed in stainless steel to create a solid, cylindrical magnetic core.[16, 17] The magnetic core was then placed in a housing with a substrate that consists of stainless steel wool which surrounds the cylindrical core and the aerosol flowed along the exterior of the magnetic core through a stainless-steel wool substrate. This configuration makes it difficult to insert the stainless-steel wool substrate and also to remove it for subsequent chemical analysis. In the present work, we have re-designed the collector so that the magnet is a hollow cylinder as shown in Figure 1, rather than a solid core. This configuration makes it much easier to change the matrix foam substrate and simplifies subsequent chemical analysis.

The outer diameter of the hollow cylinder core is 2.54 cm and the inner diameter is 1.27 cm (see Figure 1b). The total weight of the collector is approximately 581 g. As shown in Figure 1, the aerosol flows down the center of the magnetic core through the interior rather than along the exterior as in previous versions.[17] There is only one opposing pair of magnets in this configuration instead of two as in the earlier arrangements, i.e., one-stage HGPMS vs 3-stage HGPMS in Cheng et al.[17] Similar to past versions, the permanent magnets that make up the magnetic collector were made of NdFeB with a strength classified as N52 according to industry standards. The maximum magnetic field density at the location of opposing poles was estimated to be 0.2 T with no matrix substrate inserted. This number was consistent with the simulated result presented in Section 2.5. We did not calculate the maximum magnetic field of the high-gradient magnetic field with the insert added. Because of the new design of the magnetic collector, the matrix substrate can now be placed inside the magnetic core to create an interior high-gradient field, which makes the matrix application simpler and allows for different matrix materials to be manufactured in the future. The new magnetic array design and form factor was meant to reduce the overall physical dimensions, weight, operational performance (e.g., user friendliness, rapid deployment and field exchange of substrates, etc.), and logistics of the collector to make it more portable and easier to use, particularly for airborne platforms.

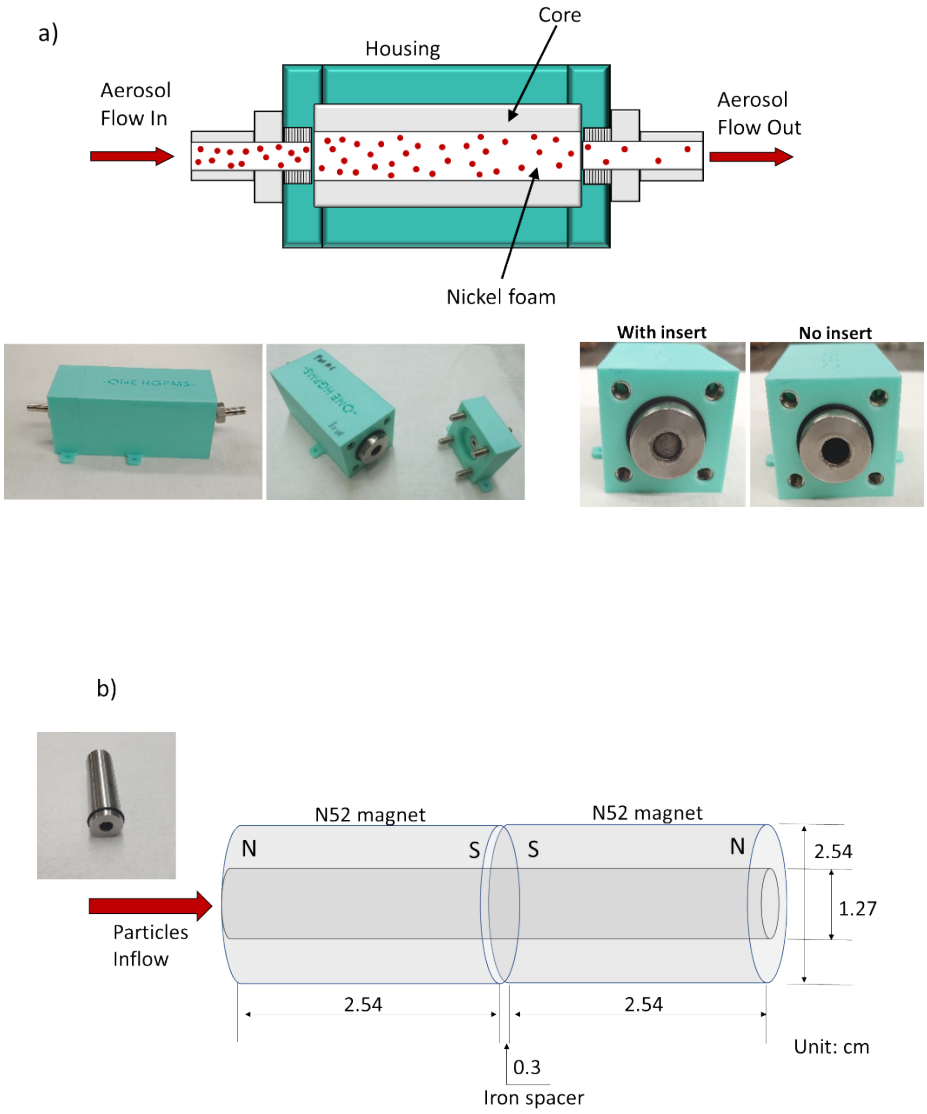

Figure 1. a) Schematic of the new HGPMS collector. The outer dimension of the housing was approximately 10.2 cm x 5.1 cm x 5.1 cm. The magnetic hollow cylinder fits inside the housing and the airborne particles are transported through the center of the cylinder. Pictures of the collector with the magnet are also shown. b) Schematic of the magnet configuration and dimension of the core (not to scale). The magnetic core of the collector is shown in the picture.

The magnetic collector shown in Figure 1 without any type of matrix insert is designated as the Permanent Magnetic Aerosol Collector (or PMAC) throughout this paper. In order to isolate the effect of the magnetic field, results from the PMAC were compared to results from a second collector with identical physical dimensions but which was constructed using non-magnetic aluminum. The aluminum collector without a matrix insert is designated as the non-magnetic aerosol collector (or NMAC) hereafter. A ferromagnetic nickel foam (MTI Corp., 99.99% purity, 1.6 mm thick) shown in Figure 2 was used as the matrix insert in both collectors. The nickel foam, which has a fiber size of approximately 100 μm and

a porosity of greater than 95%, was rolled into a rod to create the matrix for the collectors. Aerosol collection was measured for four different configurations: a) the permanent magnet with no nickel (PMAC), b) the permanent magnet with the nickel foam (PMAC-foam), c) the aluminum, or non-magnetic, collector with no nickel (NMAC), and d) the non-magnet with the nickel foam (NMAC-foam).

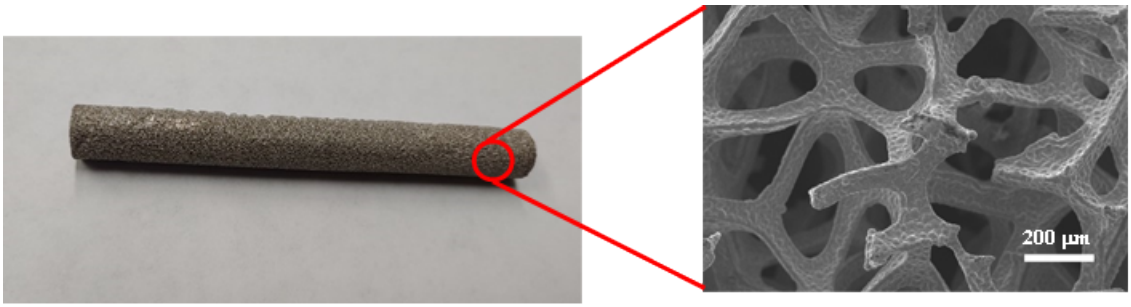

Figure 2. Photograph and SEM image of the nickel foam (MTI) used as the matrix in the collector. The framework of the nickel foam has a diameter of approximately 80 µm.

2.2 PRODUCTION OF AEROSOL PARTICLES

Three different types of particles were chosen (ferromagnetic Fe_3O_4, non-magnetic SiO_2 and diamagnetic NaCl) to investigate the impact of the new collector design on particle collection. The magnetic susceptibility for SiO_2 is -2.96×10^{-5} $cm^3\cdot mol^{-1}$, NaCl is -30.2×10^{-6} $cm^3\cdot mol^{-1}$, and Fe_3O_4 is $>7.18\times10^{-3}$ $cm^3\cdot mol^{-1}$ showing that SiO_2 and NaCl are practically non-magnetic while the Fe_3O_4 is ferromagnetic. Two different particle size regimes were used to examine the effect of particle size, nanosized particles less than 200 nm and supermicron particles of 1-2 µm. In the nanometer regime, non-magnetic NaCl particles and magnetic Fe_3O_4 (denoted as n-Fe_3O_4) particles were generated using a BGI Collison nebulizer and aqueous solutions of NaCl (0.1% w/v) or n- Fe_3O_4. The n-Fe_3O_4 nanoparticles used in the BGI nebulizer were synthesized through biogenic synthesis using akaganeite (ß-FeOOH) as a precursor. A detailed description of the synthesis of these particles is given in Cheng et al.[17]

In the supermicron regime, Fe_3O_4 (Goodfellow, FE596010, 99.9% purity, 50 µm) and SiO_2 (Cospheric, SiO2MS-2.0 1.18 µm) aerosols were generated using a fluidized bed aerosol generator (TSI, Model 3400A). Note that the source of the supermicron Fe_3O_4 aerosol particles generated by the fluidized bed was different than the nanosized Fe_3O_4 aerosol particles generated by the nebulizer. Dry, HEPA-filtered air flowed at 14 SLPM into the fluidized bed generator through a horizontal screen and created a fluidized bed of bronze beads that de-agglomerated the source powder. Approximately 25 g of Fe_3O_4 powder was placed in the source holder and transported to the fluidized bed using a chain. The generator was initially run for 2 hours prior to beginning experiments to allow for stable aerosol production. The silica aerosol was generated in a similar manner as the micron-sized Fe_3O_4 particles using the fluidized bed aerosol generator.

2.3 METHOD FOR THE COLLECTION OF NANOSIZED AEROSOLS

The experimental arrangement to measure the collection efficiency of the magnetic separator for the nanosized (<200 nm) NaCl and n-Fe_3O_4 aerosols generated by the nebulizer is shown in Figure 3. The experimental arrangement to measure the supermicron particles was slightly different and is shown in Section 2.4. For the nanosized particles, the aerosol from the nebulizer could be directed to the collector or to a bypass, which consisted of a stainless-steel tube of identical length and diameter as the collector. The bypass was used as a convenient way to measure the number concentration entering the collector. To ensure that the bypass accurately represented the aerosol at the entrance of the magnetic and non-magnetic collectors (top leg and bottom leg in Figure 3), we first measured the size distribution of the aerosol directly from the diffusion dryer and compared that distribution to one taken through the bypass. The two distributions were the same within the uncertainty of the measurement confirming that the bypass measurement accurately represented the concentration at the collector inlet. The particle size distribution was measured using a TSI scanning mobility particle sizer (SMPS, TSI Model 3080) equipped with a long differential mobility analyzer (DMA TSI Model 3081) and a nanowater condensation particle counter (WCPC TSI Model 3788). The SMPS was programmed to operate at a sheath-to-aerosol flow ratio of 10 (sheath flow = 6 LPM, aerosol flow = 0.6 LPM) with an up-scanning time of 150 s and down-scanning at 30 s. A TSI Model 3088 soft X-ray (<9.5 keV) aerosol neutralizer was used to neutralize the particles, producing bipolar ions capable of charging an aerosol particle concentration up to 10^7 cm^{-3}. The particle collection efficiency of the magnetic collector was obtained by comparing the particle size distributions and concentration through the collector to that through the bypass. Size distributions were measured through each collector and the bypass separately. For example, when measuring the size distribution through the magnetic collector, valves 1 (V1 in Figure 3) and 2 (V2) were closed to prevent flow through the bypass and the non-magnetic collector. The flow rate through the collector was 0.6 LPM (velocity of 7.9 cm/s) resulting in a residence time of 1.2 s and was essentially determined by the SMPS.

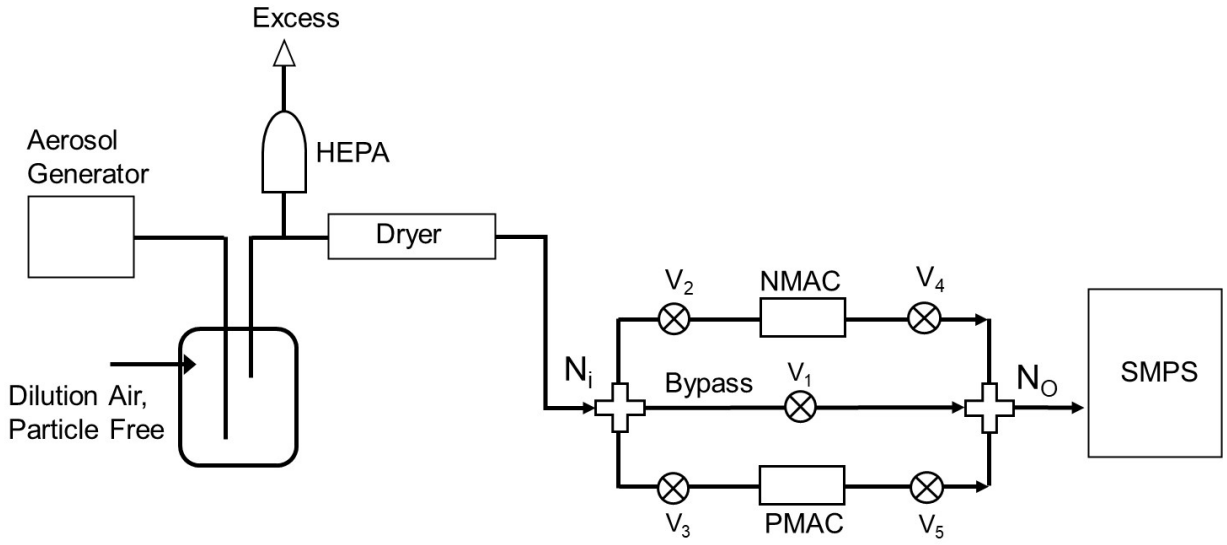

Figure 3. Diagram of the test system used to measure the collection efficiency of the magnetic collector for small particles. NMAC is the non-magnetic collector while PMAC is the magnetic collector. Valves were used to control the flow direction.

2.4 METHOD FOR THE COLLECTION OF SUPERMICRON AEROSOLS

The experimental arrangement to measure the size distributions for the supermicron particles (shown in Figure 4) was slightly different than the arrangement for the nanosized particles. The flow rate of the aerosol through the collector (or bypass) was 5 LPM as determined by an integrated pump of the APS (which pumps at 5 LPM) with the valve to the mechanical pump closed (V3). The velocity of the aerosol through the collectors was 65.8 cm/s. Excess flow exited the system through the HEPA filter thereby causing no back pressure on the collectors and or downstream aerosol instruments. After exiting either the bypass or the collector, the particle size distribution was measured using an aerodynamic particle sizer (APS, TSI Model 3321) for the micron-sized test particles.

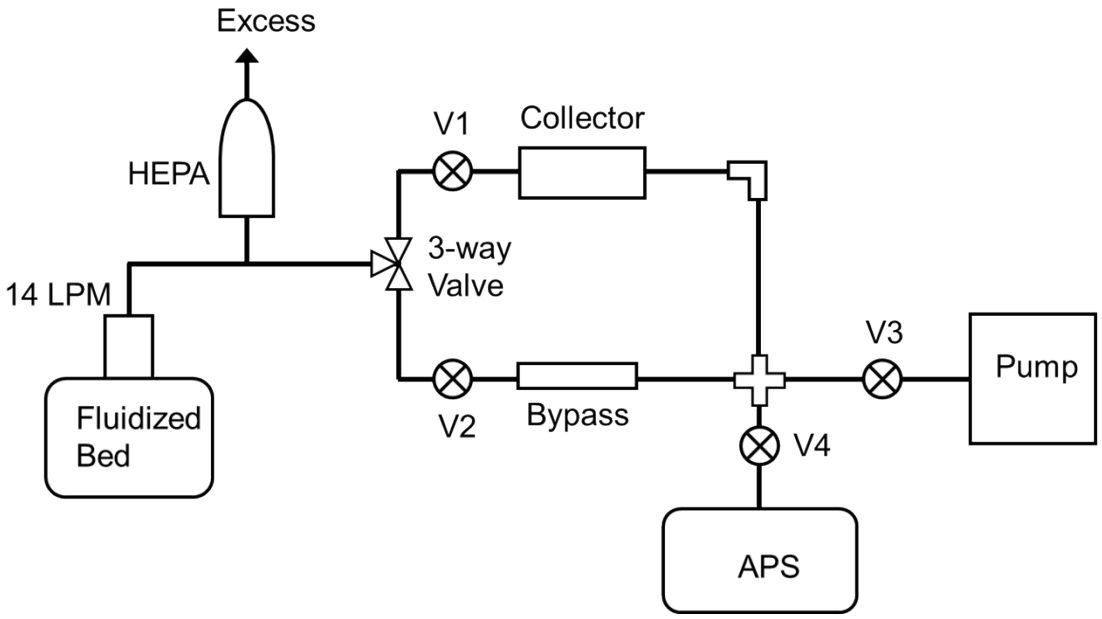

Figure 4. Diagrams of the test system used to measure the collection efficiency of the magnetic collector for supermicron particles.

2.5 MODELING THE MAGNETIC FIELD FLUX DENSITY DISTRIBUTION OF THE MAGNETIC CORE OF THE SINGLE-STAGE ASSEMBLY

The magnetic flux density B of the magnetic core implemented in the single-stage assembly of the permanent magnet pair can be described by the steady-state Maxwell equation

$$-\nabla \cdot (\mu_0 \nabla V_m - \mu_0 M_0) = 0 \quad (1)$$

where μ_o is the magnetic susceptibility, V_m is magnetic scalar potential and M_o is remanent magnetic flux. ∇ is the Laplacian operator. Eq. (1) was solved by using the Finite Element Method (FEM) in the COMSOL® ACDC module with the no current mode. An adaptive mesh (i.e., the computational grid size and grid pattern) was used with an extra-fine mesh utilized for the magnetic core and a coarser mesh for the air enclosure of the magnetic core.

Figure 5 shows the modeled magnetic flux density of the single-stage magnetic core assembly and the modeled magnetic flux direction of the assembly indicating the direction of the magnetic force. The maximum magnetic field density was approximately 0.2 T at the positions of the opposing-pole magnet pair and decreased in the axial direction to about 0.02 T at 1 cm distance away from the maximum. The enhancement of the magnetic field density in the location was approximately 10 times greater than without the opposing pair configuration. Note that the gradient of the magnetic flux density could be even higher at the edge of the matrix fiber when the foam is inserted. The flux density vector goes perpendicular to the aerosol flow axis, and therefore the resultant inward force field would favor the magnetic migration of the particles toward the collection matrix substrate filled and positioned in the center of the magnetic core. Therefore, if there is no collection matrix medium inserted in the assembly, the particles would more easily penetrate the collector.

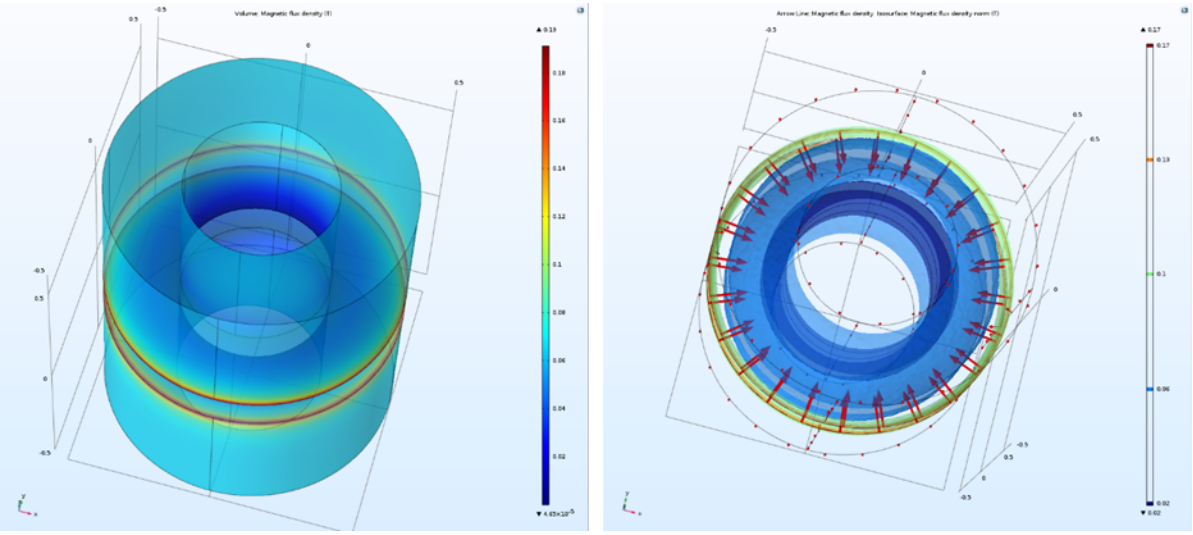

Figure 5. (Left) shows the modeled magnetic flux density of the single-stage magnetic core assembly, while (Right) displays the modeled magnetic flux direction of the assembly indicating the direction of the magnetic force.

3. RESULTS AND DISCUSSION

3.1 COLLECTION EFFICIENCY

The performance of the magnetic separator is defined as the fraction of particles removed (ζ) from the total number of particles entering the collector by using the following equation:

$$\zeta = 1 - \frac{No}{Ni} \tag{2}$$

where N_i is the number concentration at the collector inlet (in units of $\#\cdot cm^{-3}$) and N_O is the number concentration of particles escaping from the outlet of the collector. The collection efficiency is calculated as 100 * ζ (the penetration efficiency as in percentage), while ζ has no units. As mentioned, we used the bypass as the number concentration at the inlet, N_i, to calculate collection efficiencies.

3.2 COLLECTION EFFICIENCIES FOR NANOSIZED PARTICLES

Figure 6 shows the size distributions of the NaCl and n-Fe_3O_4 particles through the bypass as well as through the NMAC and PMAC at a flow rate of 0.6 LPM. The NaCl aerosol has a geometric mean of 49.3 ± 3.2 nm with a geometric standard deviation (GSD) of 1.63. The n-Fe_3O_4 showed a similar distribution with a geometric mean of 47.9 ± 1.1 nm and a GSD of 1.65. The size distribution through the bypass was very similar to the distributions through the NMAC and PMAC for both particle types showing that there was very little loss of particles through the collectors in the absence of a matrix insert. The results suggest that the force exerted on the particles by the magnetic field in the PMAC was insufficient to remove the magnetic n-Fe_3O_4 particles even though the magnetic field gradient was enhanced by 10 times in the opposing-pole configuration.

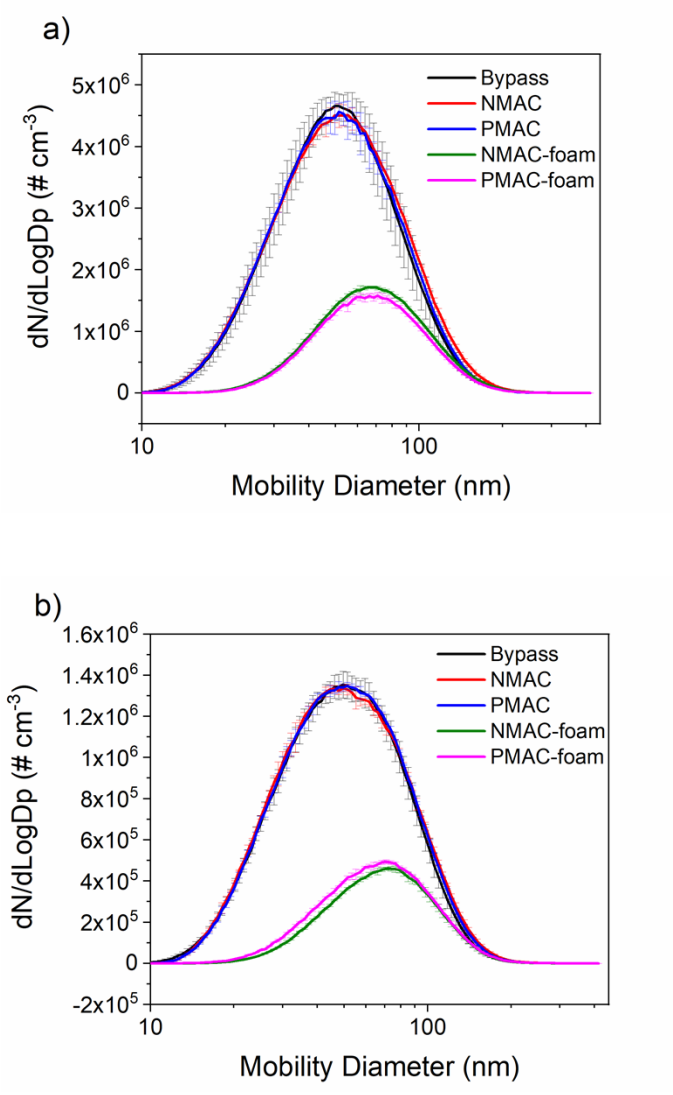

Figure 6. Pore size distributions for a) NaCl and b) Fe_3O_4 taken using the SMPS at a flow rate of 0.6 LPM. Error bars are the standard deviation from the average of multiple runs.

When the nickel foam matrix was added to both the NMAC (i.e., the NMAC-foam in Figure 6) and the PMAC (i.e., the PMAC-foam), there was a substantial reduction in the peak height of the size distributions as well as a slight shift in the peak position to a larger size indicating that the smaller size particles were preferentially removed by the foam. For the NaCl aerosol, the geometric mean shifted to 66.2 nm in the NMAC-foam and 65.6 nm in the PMAC-foam while the GSD decreased to 1.56 for NMAC-foam and 1.54 for PMAC-foam. Similarly, for the n- Fe_3O_4 aerosol, the geometric mean shifted to 66.7 nm for the NMAC-foam and 64.1 nm for the PMAC-foam while the GSD decreased to 1.53 for the NMAC-foam and 1.54 for the PMAC-foam. This shift suggests that a significant portion of smaller NaCl or n-Fe_3O_4 particles were removed by the nickel foam insert.

The collection efficiencies of the NMAC-foam and PMAC-foam were calculated using total concentration and as a function of selected sizes. The collection efficiency of the NMAC and PMAC without the nickel foam insert was nearly zero since there was no loss of particles compared to the bypass. Using total concentration as given by the SMPS, the collection efficiencies for the NaCl in the NMAC-foam and the PMAC-foam were 67%±1% and 69%±2%, respectively, which are essentially the same. This shows that the magnetic field had little effect on NaCl particle collection, which was to be expected since these particles are weakly diamagnetic. For the n-Fe_3O_4, the collection efficiency was 74%±2% in the NMAC-foam and 70%±1% in the PMAC-foam. The difference for the n-Fe_3O_4 particles appears to be statistically significant, even though the enhancement by the magnetic field did not seem to be large.

Analyzing the particle collection efficiency at selected individual sizes, we found the size dependent collection efficiencies for both the NaCl and the n-Fe_3O_4 particles as shown in Figure 7. For n-Fe_3O_4 particles less than 100 nm, the NMAC-foam slightly outperformed the PMAC-foam, though the values are very similar differing by a few percentage points, which is statistically indistinguishable. Above 100 nm, the performance was reversed with the PMAC-foam outperforming the NMAC-foam with a significant margin (> 20% for example). However, this enhanced performance for magnetic particles greater than 100 nm was somewhat weakened by the data fluctuation as reflected in the error bars due to the counting uncertainty at these larger sizes.

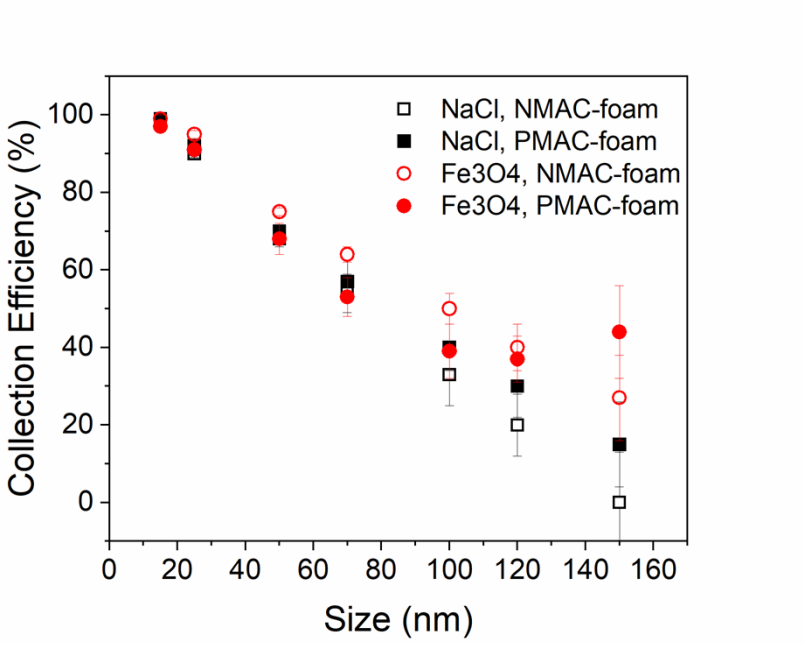

Figure 7. Collection efficiencies as a function of discrete particle size for NaCl and n-Fe_3O_4 particles. The error bars are too small to be seen for small sizes.

Lower particle concentration results in larger counting uncertainty. Because of the larger particle size, the magnetic moment of the 100 nm particles was higher than that for the smaller ones, which could lead to the higher averaged collection efficiency for the PMAC-foam.

For the NaCl particles less than 100 nm, there were no distinguishable differences in collection efficiencies between the NMAC-foam and the PMAC-foam. For those greater than 100 nm, the PMAC-foam outperformed the NMAC-foam by approximately 10%, less than that for the n-Fe_3O_4 particles. This pattern is similar to the results of the n-Fe_3O_4 particles. This similarity raises a question of why the collection efficiency for larger non-magnetic NaCl particles was also higher in the PMAC-foam than in the NMAC-foam. Was there a repulsive force on the NaCl particles as opposed to an attractive force on the n- Fe_3O_4 particles resulting in the increased collection efficiency for particles greater than 100 nm?

3.3 COLLECTION EFFICIENCIES FOR SUPERMICRON PARTICLES

The magnetic moment of larger particles and the impact on collection efficiency was investigated by using supermicron SiO_2 and Fe_3O_4 particles produced by the fluidized bed generator to test the collection efficiency of the high-gradient single-stage ring magnet assembly for larger, supermicron particles. Figure 8 shows the size distribution of the non-magnetic SiO_2 particles as produced by the generator and measured by the APS and an SEM image acquired with a JEOL SEM at a 5 kV accelerating voltage. From the SEM image, the particles are highly spherical and uniform in size. The distribution is narrow indicating good monodispersity in agreement with the manufacturer-reported coefficient of variation of 2.5% (confirming monodispersity).

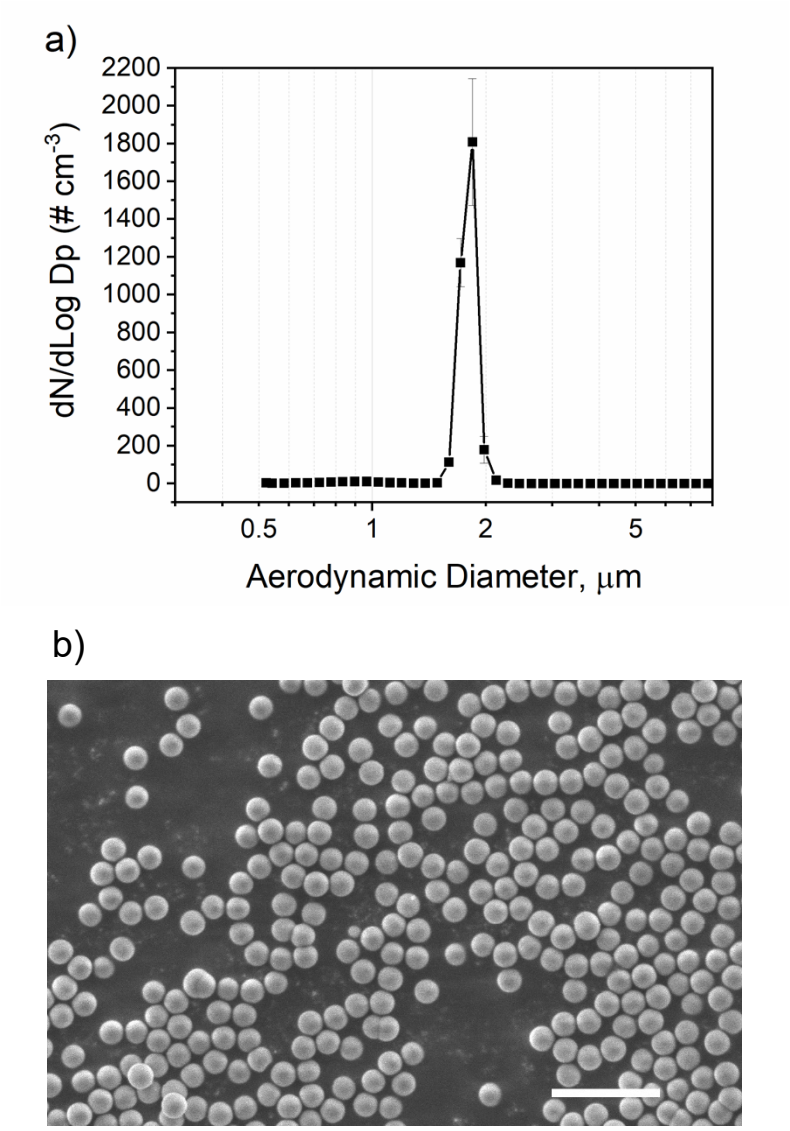

Figure 8. a) Particle size distribution of silica spheres. b) SEM image of silica spheres (scale bar = 5 μm). The flow rate through the collector was 5 LPM.

The collection efficiency of the SiO_2 particles, calculated using the total concentration from the APS, was approximately 24% in the PMAC and 23% in the NMAC (as shown in Table 1) which considering statistical variation are indistinguishable. This result is different compared to the nanoparticle results. The results for large particles show that approximately 75% of the particles penetrated the two collectors while about 25% were collected. The collections by the two devices for the non-magnetic particles were virtually the same. This result basically created a level baseline for comparing the effects of the magnetic field on supermicron particle collection. The result also indicates that the magnetic collector would perform equally well as the non-magnetic one for "non-magnetic particles."

A significant reduction in the number concentration was observed when the collection matrix (i.e., the Ni foam) was inserted into both the NMAC and PMAC. An average collection efficiency of 86% vs. 88% was estimated for the SiO_2 in the NMAC-foam and PMAC-foam, respectively (see Table 1). The increase in collection efficiency from 23% in the case of the NMAC to 86% in the case of the NMAC-foam was apparently due to the presence of the Ni foam under no external magnetic field condition. Also note that there was an increase in the average collection efficiency from 24% for PMAC to 88% with PMAC-foam suggesting that most of the silica particles were removed by the Ni foam. The use of a matrix substrate like the Ni foam adds to an average of 60+% increase in the collection of supermicron particles with or without the magnetic field. We believe the increased removal was caused by aerodynamic impaction and interception for the supermicron particles.

Table 1. Normalized collection efficiencies.

SiO_2, 1.7 μm	**No Ni**	**With Ni Foam**
NMAC	23% ± 6%	86% ± 1%
PMAC	24% ± 3%	88% ± 1%
Fe_3O_4, 1.1 μm	**No Ni**	**With Ni Foam**
NMAC	35% ± 2%	84% ± 1%
PMAC	42% ± 1%	99% ± 1%

What if the particle had magnetic components like Fe_3O_4 particles? Figure 9a shows the size distribution of the Fe_3O_4 particles produced by the fluidized bed generator with no collector present while the inset shows an SEM image of the Fe_3O_4 particles. The SEM image shows that the individual primary particles are approximately 300 – 400 nm in diameter though there was significant aggregation, which led to the aerodynamic particle size distribution of the Fe_3O_4 particles as shown in Figure 9a. The size distribution is much broader than that shown in Figure 8a indicating that the Fe_3O_4 particles are polydispersed with a peak aerodynamic diameter of approximately 1.1 μm. Figure 9b shows the size distributions measured for the NMAC and the PMAC with and without the nickel foam matrix.

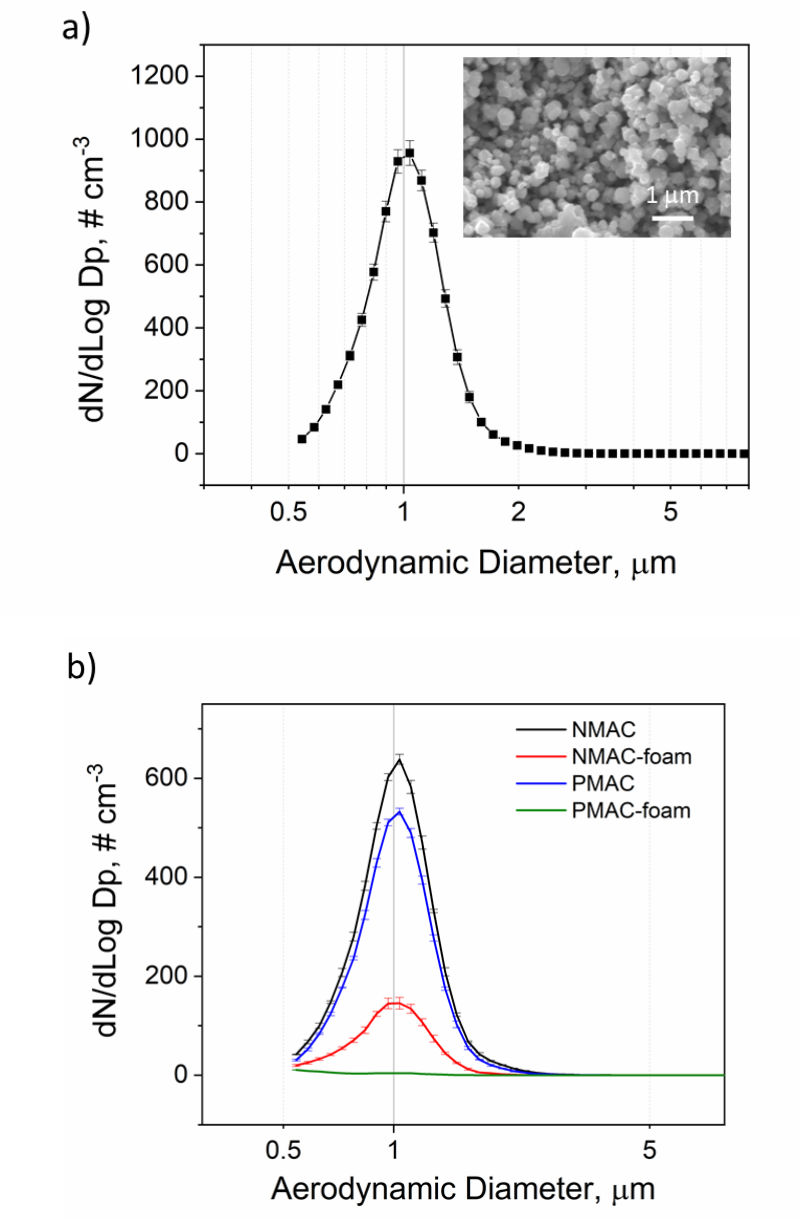

Figure 9. a) Particle size distribution of as-generated Fe_3O_4 aerosols. Inset: SEM image of Fe_3O_4 particles. b) Particle size distributions for NMAC vs. PMAC.

The collection efficiency of the supermicron Fe_3O_4 particle population was approximately 42% for the PMAC compared to 35% for the NMAC. The level of collection efficiency was higher than the silica particle data discussed earlier implying that the magnetic force present in the PMAC (without the nickel foam) did enhance the capture of the Fe_3O_4 particles by approximately 7% compared to the NMAC. This enhancement must be attributed to the larger magnetic moment of the supermicron Fe_3O_4 particles, since other variables were held constant. The 7% could therefore be improved upon if the magnetic field gradient of PMAC could be increased further or optimized.

When the collection matrix (foam) was used, the collection efficiency of PMAC-foam on Fe_3O_4 particles increased to 99% compared to 84% in the NMAC-foam. This result clearly demonstrates the effects of magnetic force on the collection of supermicron ferromagnetic particles. The Ni foam plays a critical role in the collection of the Fe_3O_4 particles, as a traditional filtration media for general particle types and an enabler for generating a high-gradient magnetic field for enhanced collection of particles that are "magnetic" in nature (e.g., ferromagnetic or possibly paramagnetic).

3.4 EFFECT OF FLOW RATE

Since the collection efficiency could vary when the incoming velocity of particles are changed, we investigated the effects of flow rate. The flow rate could change during the collection for example when the flying speed of the airborne collection platform is altered. The collection efficiency for the Fe_3O_4 particles was measured at a higher 10 LPM flow to examine the effect of flow rate on particle collection. The flow rate through the NMAC and PMAC was modified using an additional pump as shown in Figure 4. To generate 10 LPM flow through the collector, the flow to the mechanical pump was adjusted to 5 LPM using a needle valve while the integrated pump in the APS pulled 5 LPM giving a total of 10 LPM. Both valves V3 and V4 were opened to obtain the flow rate. The flows were checked prior to measurements using a DryCal DC-Lite. Note that the two flow rates correspond to flow velocities of 65.8 cm/s (5 LPM) and 131.6 cm/s (10 LPM). Measurements were then acquired for the PMAC and NMAC with and without the nickel foam matrix as was done for the 5 LPM.

The collection efficiencies at 65.8 cm/s (5 LPM) and 131.6 cm/s (10 LPM) are shown in Figure 10. Interestingly, at the higher flow velocity, the collection efficiency for the PMAC was nearly identical to the NMAC (both at approximately 32%) which is somewhat different than the lower flow velocity where the PMAC was higher at 42% compared to the NMAC at 35%. Thus, the higher collection efficiency of the PMAC compared to the NMAC at the lower flow velocity could be attributed to the magnetic contribution. In addition, the PMAC collection has higher efficiencies at both flow rates than the NMAC collection (see Figure 10). Again, the results are attributed to the magnetic force. The collection efficiency for the PMAC-foam was approximately 99% at both flow velocities suggesting the configuration is less sensitive to the change in aerosol flow rate or velocity in the collector. Even at the 2× higher flow rate, the presence of the nickel foam in the PMAC enhanced Fe_3O_4 particle collection compared to the NMAC. This result suggests a potential scale-up application of the foam for a high-flow or high-volume collection.

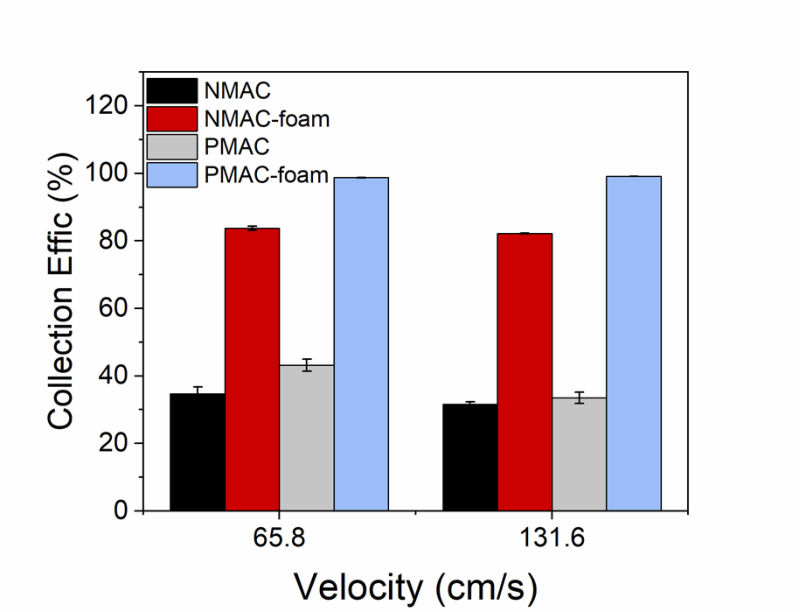

Figure 10. Comparison of collection efficiencies of the Fe_3O_4 particles at two different flow velocities (corresponding to flow rates of 5 LPM and 10 LPM).

4. CONCLUSION

In conclusion, we present the design and experimental evaluation results for a compact single-stage high-gradient magnetic particle collector for an intended use on an unmanned aerial system platform. Insertion of a nickel foam matrix into the magnetic collector enabled a high collection efficiency and robust configuration to the variation of aerosol sampling flow rate. We show that the collection efficiency of micron-size Fe_3O_4 particles in the PMAC with the nickel matrix was nearly 100% at two different flow rates. Thus, the PMAC-foam device was found to have high collection efficiency for larger particles and was able to distinguish magnetic from non-magnetic particles. Collection for small (< 0.1 microns) NaCl and n-Fe_3O_4 particles showed that both devices performed similarly with the nickel foam irrespective of particle magnetic susceptibility possibly due to the small magnetic moment of the small particles. We conclude that the single-stage PMAC-foam device has high efficiency in particle collection but was ineffective in terms of separating small particles based on their magnetic moments. Experiments at higher flow rates indicated that both the NMAC-foam and PMAC-foam technique are insensitive to the variation in aerosol sampling flow rate, but the PMAC configuration is able to distinguish magnetic from non-magnetic while the NMAC was not.

5. ACKNOWLEDGEMENTS

The research was supported by the National Nuclear Security Administration of the United States Department of Energy. Oak Ridge National Laboratory is managed by UT-BATTELLE, LLC for the U.S. DEPARTMENT OF ENERGY under contract DE-AC05-00OR22725. This work would not be possible without the advanced magnetic manufacturing skills of ORNL craftsmen and technical support. HGPMS is an ORNL-patented technology (patent # US 9,387,486). We also acknowledge the work of Bart Murphy who manufactured the test magnets used in this project and 3D printing.

6. REFERENCES

1. Watson, J.H.P. 1973. “Magnetic Filtration.” *J. Appl. Phys.* 44:4209-4213.
2. Watson, J.H.P. 1995. “Permanently Magnetized High-Gradient Magnetic Air Filters for the Nuclear Industry.” *IEEE Trans. Magn.* 31:4181-4183.
3. Oder, R.R. 1976. “High Gradient Magnetic Separation Theory and Applications.” *IEEE Trans. Magn.* 12:428-435.
4. Clarkson, C.J., D. R. Kelland. 1978. “Theory And Experimental-Verification of a Model for High Gradient Magnetic Separation.” *IEEE Trans. Magn.* 14:97-103.
5. Lua, A. C., R. F. Boucher. 1982. “An Investigation of Efficiency of High-Gradient Magnetic Gas Filtration.” *IEEE Trans. Magn.* 18:1659-1661.
6. Liu, Y. A., M. J. Oak. 1983. “Studies in Magnetochemical Engineering .3. Experimental Applications of a Practical Model for High-Gradient Magnetic Separation to Pilot-Scale Coal Beneficiation.” AIChE J. 29:780-789.
7. Ditsch, A., S. Lindenmann, P. E. Laibinis, D. I. C. Wang, T. A. Hatton. 2005. “High-Gradient Magnetic Separation of Magnetic Nanoclusters.” *Ind. Eng. Chem. Res*. 44:6824-6836.
8. Moeser, G. D., K. A. Roach, W. H. Green, P. E. Laibinis, T. A. Hatton. 2002. “Water-Based Magnetic Fluids as Extractants for Synthetic Organic Compounds.” *Ind. Eng. Chem. Res.* 41:4739-4749.
9. Boucher, R. F., O. O. Okeke. 1990. “High-Gradient Magnetic Filtration of Paramagnetic Dust Using Woven Wire Matrix.” *Aerosol Sci. Technol*. 12:300-311.
10. Lu, D. F., C. S. Zhao, X. Wu, Y. W. Li, S. Han. 2007. “Experimental Study on Capture of Pm10 Emitted from Coal Combustion with High Gradient Magnetic Field.” *AIP Conference Proceedings*, 587-592.
11. Vehring, R. 2008. “Pharmaceutical Particle Engineering Via Spray Drying.” *Pharm. Res*. 25:999-1022.
12. Schaller, V., U. Kraling, C. Rusu, K. Petersson, J. Wipenmyr, A. Krozer, G. Wahnstrom, A. Sanz-Velasco, P. Enoksson, C. Johansson. 2008. “Motion of Nanometer Sized Magnetic Particles in a Magnetic Field Gradient.” *J. Appl. Phys*. 104:14.
13. Forbes, B., B. Asgharian, L. A. Dailey, D. Ferguson, P. Gerde, M. Gumbleton, L. Gustavsson, C. Hardy, D. Hassall, R. Jones, R. Lock, J. Maas, T. McGovern, G. R. Pitcairn, G. Somers, R. K. Wolff. 2011. “Challenges in Inhaled Product Development and Opportunities for Open Innovation.” *Adv. Drug Deliv. Rev.* 63:69-87.
14. Kim, Y. G., J. B. Song, D. G. Yang, J. S. Lee, Y. J. Park, D. H. Kang, H. G. Lee. 2013. “Effects of Filter Shapes on the Capture Efficiency of a Superconducting High-Gradient Magnetic Separation System.” *Supercond. Sci. Technol*. 26:7.
15. Zadravec, M., M. Hribersek, P. Steinmann, J. Ravnik. 2014. “High Gradient Magnetic Particle Separation in a Channel with Bifurcations.” *Eng. Anal. Bound. Elem*. 49:22-30.
16. Cheng, M. D., S. L. Allman, G. M. Ludtka, L. R. Avens. 2014. “Collection Of Airborne Particles By A High-Gradient Permanent Magnetic Method.” *J. Aerosol. Sci.* 77:1-9.
17. Cheng, M. D., B. L. Murphy, J. W. Moon, G. M. Lutdka, P. R. Cable-Dunlap. 2018. “On the Use of High-Gradient Magnetic Force Field in Capturing Airborne Particles.” *J. Aerosol. Sci.* 120:22-31.

18. Yang, T., Q. S. Liu, H. X. Li, Q. L. Zeng, L. S. Chan. 2010. "Anthropogenic Magnetic Particles and Heavy Metals in the Road Dust: Magnetic Identification and its Implications." *Atmos. Environ.* 44:1175-1185.

19. Sagnotti, L., P. Macri, R. Egli, M. Mondino. 2006. "Magnetic Properties of Atmospheric Particulate Matter from Automatic Air Sampler Stations in Latium (Italy): Toward a Definition of Magnetic Fingerprints for Natural and Anthropogenic PM10 Sources." *J. Geophys. Res.-Solid Earth* 111:17.

20. Gorka-Kostrubiec, B. 2015. "The Magnetic Properties of Indoor Dust Fractions as Markers of Air Pollution Inside Buildings." *Build. Environ*. 90:186-195.

21. Baron, P. A., K. Willeke. 2005. Aerosol Measurement: Principles, Techniques, and Applications. 2nd ed.; John Wiley & Sons: Hoboken, NJ.

22. Cheng, M. D. 2018. "Selective Collection of Airborne Particulate Matter." *Aerosol Air Qual. Res*. 18:1361-1365.

23. Hsiao, T. C., P. A. Jaques, P. F. Gao. 2013. "A Multidomain Magnetic Passive Aerosol Sampler: Development and Experimental Evaluation." *Aerosol Sci. Technol.* 47:37-45.

24. Zarutskaya, T., M. Shapiro. 2000. "Capture of Nanoparticles by Magnetic Filters." *J. Aerosol. Sci.* 31:907-921.